Formation, Properties, and *"ex situ"* Soil Decontamination by Vegetable Oil-Based Microemulsions

Marcia Bragato and Omar A. El Seoud*

Instituto de Química, Universidade de São Paulo, 05513-970, São Paulo, S.P., Brazil

ABSTRACT: We have investigated soil decontamination by vegetable oil-based fluids. Methyl esters of babassu oil (BME) and the unsaturated fraction of palm oil (UPME) were prepared by transesterification of precursor oils. Phase diagrams of each fatty ester/water/nonionic surfactant (Synperonic 91/4) were studied as a function of system composition and temperature. Measurements of solution rheology, quasi-elastic light scattering, and interfacial tension were employed to demonstrate that the single phases obtained are either bicontinuous or water-in-oil microemulsions (μE). Both types were used in decontamination of three different soils, impregnated with polycyclic aromatic hydrocarbons. As decontaminators, BME- and UPME-based μE (at 37.5, and 42.5°C, respectively) are more efficient than hot toluene. This is attributed to desorption and subsequent solubilization of contaminants by the μE. The viability of this decontamination scheme is further supported by material balance. Decontamination has increased soil bio-availability.

Paper no. S1320 in *JSD 6*, 143–150 (April 2003).

KEY WORDS: Babassu oil, bicontinuous phases, *"ex situ,"* microemulsions, palm oil, soil decontamination.

The choice of a soil decontamination technique (biological, chemical, or physical) depends on several factors, e.g., the chemical structure and concentration of pollutants present, characteristics of the soil (e.g., its granulometry, porosity, and humic matter content), geology of the site, and presence of groundwater (1). Independent of the technique employed, decontamination can be *"in situ"* or *"ex situ."* The former is reminiscent of tertiary oil recovery, where the decontamination fluid is injected into the soil, usually at the site perimeter, then removed by pumping from a central location. The *"ex situ"* technique involves excavation of contaminated soil, followed by treatment either on- or off-site, and redeposition (2). This method is particularly suitable for decontamination from pollutants frequently present in dumping sites of industrial plants, e.g., polycyclic aromatic hydrocarbons (PAH) and polychlorinated biphenyls (3–5).

The efficiency of soil decontamination by washing with either water or a surfactant solution is low; post-treatment of relatively large volumes of contaminated liquids is needed (6). More recently, microemulsions (μE) have been employed as decontamination fluids. These are transparent or translucent liquids containing at least three components, namely, surfactant (S), oil (O), and water (W). They are isotropic and thermodynamically stable under *a specified set of experimental conditions.* Soil decontamination by μE is an attractive technique because of the following features: (i) Efficiency: The μE desorbs contaminants by decreasing the pollutant/soil interfacial tension to very low values (7); desorbed material then dissolves in the μE; (ii) Convenience: The volumes handled are much smaller than those produced from washing with either water or aqueous micellar solution; (iii) Viability of recycling: Separation of the μE into two phases is trivial, and the aqueous phase is recycled into the process (see below).

A recently introduced *"ex situ"* soil decontamination process involves the following steps: (i) extraction of the contaminated soil with the μE; (ii) separation of the soil from the μE; (iii) temperature-induced separation of the μE into two phases: an oil-rich phase, containing dissolved pollutants, and a surfactant-rich aqueous phase; (iv) disposal of the oil-rich phase (e.g., by biological treatment or incineration) and recycling of the surfactant-rich aqueous phase into the process; (v) washing and redeposition of treated soil (8–10). Environmental considerations dictate that components of μE should be biodegradable, this being the reason for using vegetable oils, not mineral ones.

Application of the above-mentioned decontamination scheme requires an understanding of the contribution of the following variables to the formation and stability of μE: (average) structure of the vegetable oil, composition of the μE, and temperature. A recent study has shown that methyl esters of coconut oil (CME) and the saturated fraction of palm oil (SPME) form μE that can be used to decontaminate oil (11). We report here on the formation, properties, and soil decontamination by μE based on other, more unsaturated vegetable oils, namely, methyl esters of babassu oil (BME) and methyl esters of the unsaturated fraction of palm oil (UPME). Attractive characteristics of decontamination by these μE include high efficiency, fast soil extraction, and favorable material balance.

*To whom correspondence should be addressed at Instituto de Química, Universidade de São Paulo, C.P. 26077; 05513-970, São Paulo, S.P., Brazil. E-mail: elseoud@iq.usp.br

Abbreviations: BME, babassu oil methyl esters; CEC, cation exchange capacity; CME, coconut oil methyl esters; EO, oxyethylene; IFT, interfacial tension; μE, microemulsion; O, oil; PAH, polycyclic aromatic hydrocarbons; PIT, phase inversion temperature; QELS, quasi-elastic light scattering; S, surfactant; SPME, methyl esters of the saturated fraction of palm oil; θ, contact angle; UPME, methyl esters of the unsaturated fraction of palm oil; UV-vis, ultraviolet-visible; W, water.

EXPERIMENTAL PROCEDURES

Materials

All reagents were purchased from Aldrich or Merck and were purified as given elsewhere (12). Food-grade babassu oil (*Orbygnia speciosa*) and palm oil (*Elaeis guineensis*) were purchased from Campestre Óleos Vegetais (S.B. Campo, São Paulo, Brazil). Chromatographic standards for analysis of the fatty acid composition were from Polyscience (Niles, IL).

The commercial nonionic surfactants tested were Synperonic 91/4 (REO_4), and Synperonic 91/5 (REO_5), where R = $CH_3(CH_2)_{8/10}$ and EO refers to an oxyethylene unit (ICI, Middlesborough, United Kingdom). Both surfactants are blends, with R = 35% $CH_3(CH_2)_8$– and 65% $CH_3(CH_2)_{10}$– (determined by high-performance liquid chromatography; Haegel, F.-H., personal communication). Tonsil Optimum 210FF (a Ca-bentonite clay; Süd Chemie, Munich, Germany), and Merck silica gel 60 A were used as received. Their specific areas are 210 and 100 m^2g^{-1}, respectively.

Three type of PAH-contaminated soils were used: (i) One obtained from Forschungszentrum Jülich (Jülich, Germany, hereafter designated as "contaminated soil"). Its organic matter and PAH contents were found to be 13.5%, and 3600 ppm (Soxhlet extraction with toluene, 6 h), respectively; (ii) artificially-contaminated Tonsil 210FF; and (iii) silica gel (the latter two hereafter designated as "contaminated bentonite" and "contaminated silica," respectively). The latter samples were doped with 400 or 3600 ppm pyrene, as follows: Solid pyrene was dissolved in a suspension of the adsorbent in ethanol (0.1 g/mL). The suspension was mechanically stirred for 12 h, left to stand for 48 h, and the solvent was then evaporated at 45°C, under reduced pressure.

Preparation and Characterization of BME and UPME

These were prepared by transesterification (sodium methoxide/methanol) of the appropriate oil (13,14). Palm oil methyl esters were then separated into an unsaturated-rich fraction, UPME, and a saturated-rich one, SPME, as follows: The mixture obtained was centrifuged at 4.0 ± 0.1°C, at 4280 × *g* for 30 min. The liquid fraction that separated (UPME) was bleached by heating (2 h at 40°C) with 0.5% (wt/vol) of Tonsil 210FF clay.

The esters obtained were kept refrigerated (*ca.* 5°C), under nitrogen, in tightly stoppered polyethylene bottles, and were characterized by the following American Oil Chemists' Society official methods: moisture, Ca-2e-84; acid value, OM Cd 3a-63; iodine value (Wijs), OM RP Cd 1b-87; peroxide value, OM Cd 8-53; saponification value, OM Cd 3-25; fatty acid composition, OM Ce 1-62 (GC analysis) (15). The latter was carried out with a Shimadzu model GC 17A-2 gas chromatograph (Kyoto, Japan), as given elsewhere (11).

Phase Diagrams

Surfactant, water, and the methyl esters (hereafter designated as "oil") were accurately weighed in Pyrex tubes, provided with Teflon-lined caps. The contents were thoroughly mixed, then thermostated until phase equilibrium was reached (several hours to days). The number and appearance of phases was noted (using crossed polarizers to detect liquid crystalline phases). The tubes were then submitted to another cycle of mixing/thermostating at a new, lower temperature. We used 5°C intervals, or 2.5°C intervals when there was a change in the number of phases (16,17). The main component of each phase, W or O, was determined by use of dyes, as given elsewhere (11).

Characterization of the Monophases

The following techniques were employed to characterize the monophases formed: rheology, quasi-elastic light scattering (QELS), interfacial tension (IFT), and contact angle, θ.

Rheological Measurements

The viscosities and rheological behavior of the pure components (O and S) and the monophases were studied as a function of temperature, 35.0 to 45.0 ± 0.1°C; time, 0 to 6 min; and shear rate, 75 to 450 s^{-1} with model LV-III, cone/plate rheometer (Brookfield, Stoughton, MA).

QELS

We used a model 4700MW LS system (Malvern, Worcestershire, United Kingdom), equipped with a He/Ne laser source (Spectra Physics, Mountain View, CA). The sample was directly filtered into the measurement cell (0.45 μm filter) and left for 15 min for thermal equilibration. Treatment of the scattered intensity by the cumulants method was employed to calculate the apparent D and the normalized diffusion coefficient D_n, as given elsewhere (11,18,19).

IFT Measurements

A site-4 spinning-drop tensiometer (Krüss, Hamburg, Germany) was employed. After phase separation at the desired temperature, the appropriate two-phase system was inserted in the capillary tube of the equipment and allowed to re-equilibrate thermally. Its IFT was then measured (20).

Contact Angle

After phase separation at the desired temperature, the advanced contact angle (±2°) of the μE drop (8 μL) was measured as recommended elsewhere (21), with a home-built apparatus equipped with a QV-10 LCD digital camera (Casio, Tokyo, Japan). The glass slide employed was cleansed as recommended elsewhere (22).

Physical Characterization of Soils Employed

The following techniques were employed for soil characterization: mineral composition, X-ray diffraction, Phillips model X'pert MPD X-ray diffractometer; granulometry, Malvern Sedigraph Mastersizer/E, an aqueous suspension of the soil (0.5 g/L) was magnetically stirred for 8 h, with-

out a deflocculant, then immediately analyzed; surface area, BET method (23), ASAP 2010 BET porosimeter (Micromeritics Equipment, Norcross, GA), according to ASTM designation B4567/94. Measured specific surface areas were 8.8, 210, and 100 m^2g^{-1} for contaminated soil, Tonsil Optimum 210FF, and silica gel 60 A, respectively.

Kinetics of Decontamination

The decontamination rate constant was determined at a μE/silica ratio of 6:1 (w/w). Glass vials, each containing a known weight of the μE, were thermostated at 37.5°C. The required weight of artificially contaminated silica (pyrene, 400 ppm) was added to each vial; the mixture was thoroughly agitated for 30 s, then left in the thermostat for the required contact time. The suspension was quickly filtered (by suction) directly into a 10-mL volumetric flask. The silica was washed three times, each with 2 mL of anhydrous ethanol. Solution volume was made up to the mark with ethanol, and the pyrene concentration was determined as given below. Pseudo first-order rate constants, k_{obs}, were calculated from the (linear) plot of log ($[pyrene]_\infty - [pyrene]_t$) vs. contact time. The latter was calculated from mixing until the start of filtration. Triplicate runs agreed within ±5%.

Soil Decontamination by Microemulsions: Capacity of Extraction of PAH

Pre-prepared μE was added to contaminated soil; the contents were thoroughly mixed for 2 min and then left at a constant temperature for the required contact time. The contents were centrifuged at 4280 × *g* for 15 min, then the PAH concentration was determined in the supernatant from its absorbance at λ = 333.5 nm [Beckman DU-70 ultraviolet-visible (UV-vis) spectrophotometer]. A Beer's law plot was based on the solid obtained by exhaustively extracting contaminated soil with hot toluene (6 h, Soxhlet). Anhydrous ethanol was used as solvent. The same procedure was applied to contaminated bentonite and/or silica, except that the pyrene concentration was calculated from the appropriate Beer's law plot.

Properties of Decontaminated Soil

After soil/supernatant separation, the former was stirred with water for 2 h (water/soil ratio = 10, w/w) then centrifuged at 4280 × *g* for 30 min. After two more washings, the soil was dried under reduced pressure at room temperature to a constant weight. Its surface area was determined by the BET method (23), whereas its cation exchange capacity (CEC) was determined by the methylene blue adsorption method (24).

Material Balance

Contaminated silica (3600 ppm pyrene) was treated with the BME-based μE as given in the section on soil decontamination. The solid was filtered off, the single phase was separated into two phases by lowering its temperature, and the components of each phase were analyzed by the following methods: pyrene, UV-vis; water, Karl Fischer titration; BME, gas chromatography; nonionic surfactant, ^1H nuclear magnetic resonance spectroscopy (Bruker DRX-500 spectrometer).

BME in the aqueous phase was extracted twice with hexane and was quantified after solvent removal. Surfactant concentration in the aqueous phase was determined as follows: A sample (from the oil and/or the aqueous phase) was dried under reduced pressure, and the residue was dissolved in CD_3Cl and analyzed. Surfactant concentration was determined by comparing areas of the peaks at 3.584–3.723 (EO units) and 2.616 ppm (dimethylsulfoxide internal reference).

RESULTS AND DISCUSSION

Choice of System Components

Soil decontamination by systems of single components is prohibitively expensive. "Single components" designates systems where the oil is a single compound, e.g., methyl laurate, and the nonionic surfactant is chromatographically pure, e.g., $C_{12}H_{25}EO_4$. Therefore, we used methyl esters of two vegetable oils and commercial nonionic surfactants.

Palm oil is the second-most produced oil worldwide, after soybean oil (25). In Brazil, it is produced mainly in the north and northeast regions. The babassu tree grows in the Amazon region, where most of the production is still from native areas, especially in the state of Maranhão (26). The characteristics of these oils, along with CME and SPME, are listed in Table 1. The latter shows that the oils employed in the present study have longer (average) chain lengths and are more unsaturated than those previously employed (11). Both factors could affect phase boundaries and compositions of the μE because of differences between penetration of saturated and unsaturated oils into the O/W interface (27).

TABLE 1
Comparative Characteristics of the Methyl Esters of Coconut Oil (CME), Babassu Oil (BME), and the Saturated (SPME) and Unsaturated (UPME) Fractions of Palm Oil

Analysis[a]	CME[b]	BME	SPME[b]	UPME
Fatty acid composition (%)[c]				
C8:0	7.7	4.4		
C10:0	5.2	3.2		
C12:0	47.0	50.4		0.1
C14:0	19.6	15.0	0.5	0.6
C16:0	9.9	7.3	56.6	37.4
C18:0	1.0	2.0	5.0	3.7
C18:1Δ^9	7.1	15.2	30.7	47.1
C18:2$\Delta^{9,12}$	2.5	2.5	7.2	10.8
C20:0	—	—	—	0.3
Ave. carbon no.[d]	13.7	14.2	16.8	17.1
Saponification number	240	231	215	208
Acidity value	0.2	0.02	0.5	0.8
Iodine value (mg KOH/g sample)	11.6	17.0	16.3	56.2
Peroxide value (mequiv/kg sample)	1.2	1.5	1.8	18.3

[a]Official and recommended American Oil Chemists' Society methods. (15).
[b]Data taken from Reference 11.
[c]Normalized values.
[d]Calculated from the composition of fatty acids and their molecular weights.

The general structure of a nonionic surfactant is C_iEO_j, where the subscripts *i* and *j* refer to the average number of carbon atoms in the surfactant hydrophobic chain and the average number of EO units in its hydrophilic moiety. We employed nonionic surfactants because (i) μE can be obtained with only three components, namely, W, O, and S; (ii) their hydrophilic-lipophilic balance can be adjusted by the appropriate combination of *i* and *j*; and (iii) the phase diagram is governed by both the temperature and the change in spontaneous curvature of the interfacial surfactant film (28,29). The reason for employing $C_{9/11}EO_4$ instead of $C_{9/11}EO_5$ will become apparent shortly.

The contaminated soil employed is a typical difficult-to-handle montmorillonite: It is highly contaminated (3600 ppm PAH); its organic matter content is relatively high (13.5%); and its average granulometry is very small, 90% < 50 μm, and 50% < 10 μm. Additionally, we investigated two other soils, namely, contaminated bentonite and silica.

Phase Diagrams

Consider the phase behavior that is typically observed for systems of single components, e.g., O(dodecane)/W/S($C_{12}H_{25}EO_4$). At constant pressure, the system is specified by setting three independent variables, namely, the temperature, *T*, and two composition variables, α and γ, which are conveniently defined (17,19,30) as:

$$\alpha = O/(O + W) \quad [1]$$

$$\gamma = S/(S + O + W) \quad [2]$$

where the concentration of all components is given in weight. If α is fixed, e.g., at 0.5, then the resulting pseudo-binary phase diagram (between *T* and γ) has the appearance of a "fish," with "body" and "tail" that meet at a composition designated as $\tilde{\gamma}$, and a temperature (the phase inversion temperature: PIT) designated as $\tilde{T}$ (see Fig. 1A). At a fixed γ (below 0.4 in Fig. 1A), an increase in *T* causes a change in the number and nature of phases from a two-phase system, $\underline{2\phi}$, in which the O/W μE is in equilibrium with the excess oil phase, to a three-phase system, 3ϕ, in which a bicontinuous phase is in equilibrium with both oil-rich and water-rich phases, to another two-phase system, $\overline{2\phi}$, in which the W/O μE is in equilibrium with the excess water phase. The region covered by the "fishtail" corresponds to a one-phase system (1ϕ). At $\tilde{T}$, the surfactant has equal solubilities in O and W, and the system is a bicontinuous phase (surfactant film with zero spontaneous curvature). A liquid crystalline phase, Lα, may also be observed at higher γ (30).

Figure 1B shows that the phase diagrams of BME/W/$C_{9/11}EO_5$ and BME/W/$C_{9/11}EO_4$ have similar shapes, except that the 1ϕ region forms at a higher temperature for the former surfactant. The solubility of a nonionic surfactant, C_iEO_j, in water increases as a function of increasing *j*, at a constant *i* (31). Consequently, $\tilde{T}$ increases, in agreement with Figure 1B. For soil decontamination, therefore, $C_{9/11}EO_4$ is the more interesting surfactant; it was used in the rest of our study.

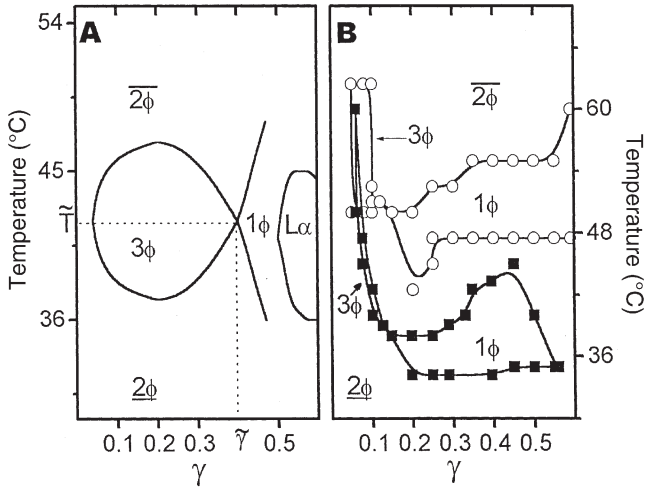

FIG. 1. Phase diagram for (A) the system of single components, redrawn from Reference 30 and showing the "fish" with its "body" and "tail." In this figure, the phase symbols are 1ϕ $\underline{2\phi}$, $\overline{2\phi}$, 3ϕ, Lα, and E. They refer, respectively, to one phase, oil-in-water (O/W) microemulsion (μE) in equilibrium with excess oil phase, W/O μE in equilibrium with excess water phase, oil-rich and water-rich phases in equilibrium with a bicontinuous phase, lyotropic liquid crystalline phase, and emulsion. $\tilde{T}$ is the phase inversion temperature. The composition variables are α = O/(O + W) and γ = S/(S + O + W), where S = surfactant, and O, W, and S are given in weight. The type of each phase is indicated within the corresponding area. (B) Phase diagrams for the systems BME/$C_{9/11}EO_5$/water, (○); and BME/$C_{9/11}EO_4$/water (■), where BME = babassu oil methyl esters, $C_{9/11}$ = $CH_3(CH_2)_{8-10}$, and EO = oxyethylene.

Dependence of Phase Diagrams on the Structure of Oil

Relationship between γ and T. Figure 2 shows the relationship (pseudo-binary phase diagrams) between γ and *T* at two fixed α, 0.5 and 0.9, for BME and UPME, respectively. The qualitative differences between the phase diagrams shown in Figures 1A (system of single components) and 2 include: distortion of the fish-type diagrams; separation of the two 1ϕ regions by Lα in equilibrium with μE (at α = 0.5); and formation of stable emulsions at lower γ.

These differences are not surprising, because the number and nature of phases depend on the distribution of surfactant between O and W. When multicomponent systems are used, the conditions for the formation of, e.g., a 3ϕ region are not easily attainable because of the distribution of a series of surfactants, each with its own PIT, between water and a series of oil components, each with a different number of carbon atoms. This results in severely distorted fish-type phase diagrams, whose body areas are reduced compared to that depicted in Figure 1A, as shown elsewhere (31–34). $\tilde{T}$ is usually calculated as the mean of the upper and lower temperatures of the 3ϕ region. Calculation of $\tilde{T}$ from Figure 2 has proved to be untenable; QELS data have been employed, however, to obtain this information as discussed shortly.

Relationship between α and T. Figure 3 shows the so-called channel-cut in the phase diagram, i.e., the relationship between α and *T* at constant γ. Again, for comparison, part A refers to the channel-cut in the phase diagram for a system

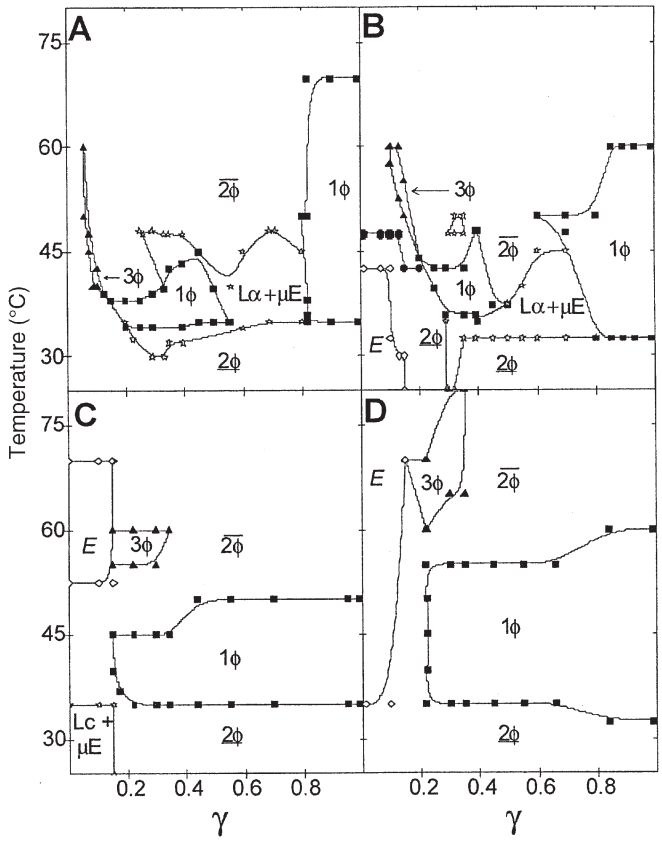

FIG. 2. Pseudo-binary phase diagrams (fish diagrams) for BME/$C_{9/11}EO_4$/water. (A) α = 0.5, (C) α = 0.9. UPME/$C_{9/11}EO_4$/water. (B) α = 0.5, (D) α = 0.9. UPME, methyl esters of the unsaturated fraction of palm oil; α = O/(O + W); Lc, liquid crystalline domain; for other abbreviations and symbols see Figure 1.

of single components, *n*-decane/W/C_8EO_4, at γ = 0.38 (16,17). The main feature of part A is the 1ϕ channel that goes from the lower left corner (O/W μE) to the upper right corner of the phase diagram (W/O μE). In contrast, parts B (BME) and C (UPME) do not show a 1ϕ system at α < 0.5 (γ = 0.3). This result can be explained by considering the effect of oil structure on its penetration into the surfactant film at the O/W interface, probably with its ester group in contact with water (27). Extensive penetration of the ester group into the surfactant film decreases the spontaneous curvature and increases the elasticity modulus of the latter. Both factors sterically constrain the curvature of the interface to favor W/O structures (35,36). That is, extensive film penetration by BME and UPME oils destabilizes O/W μE.

Probing the microstructures of the monophases. The isotropic 1ϕ region may consist of μE and/or cubic liquid crystals. Since microstructures cannot be inferred from phase diagrams alone; we employed the following techniques to address this question:

(i) Rheology. All 1ϕ regions had low viscosity and exhibited Newtonian behavior, in variance with results observed for cubic liquid crystals, which are extremely viscous and do not exhibit Newtonian behavior (37–39). This result means that QELS measurements will not be complicated, e.g., by multiple scattering from cubic liquid crystals (40) and that the low-viscosity 1ϕ systems can be conveniently employed for soil decontamination.

(ii) QELS. The dependence of D_n on temperature and α (Figs. 4A and 4B, respectively) enabled us to confirm the formation of bicontinuous phases and to calculate $\tilde{T}$. Thus, the U-shaped curve depicted in Figure 4A is qualitatively similar to that observed for bicontinuous phases of a variety of systems of single components (41,42). The vertical lines drawn refer to the limits of the 1ϕ regions, outside of which QELS measurements are precluded by solution opalescence. The minima observed result from the increase in aggregate sizes, as bicontinuous phases are approached, and are located at the PIT. Average PIT were calculated after comparing the dependence of D_n on T for all α for which

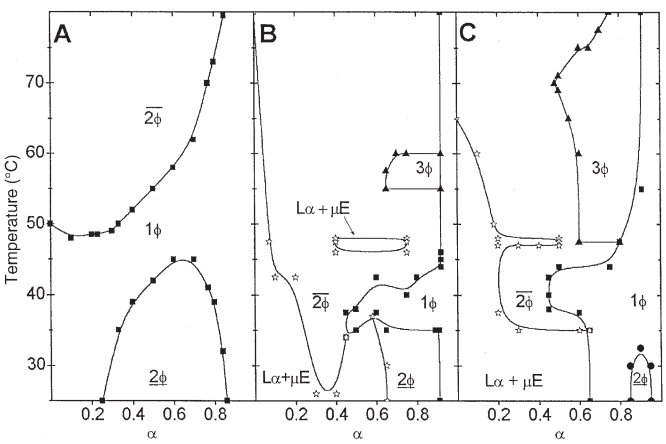

FIG. 3. Pseudo-binary phase diagrams at a constant γ (channel-cut): (A) *n*-decane/C_8EO_4/water, γ = 0.38, redrawn from Reference 17; (B) BME/$C_{9/11}EO_4$/water, γ = 0.30; (C) UPME/$C_{9/11}EO_4$/water, γ = 0.30. γ = S/(S + O + W); for other abbreviations and symbols see Figures 1 and 2.

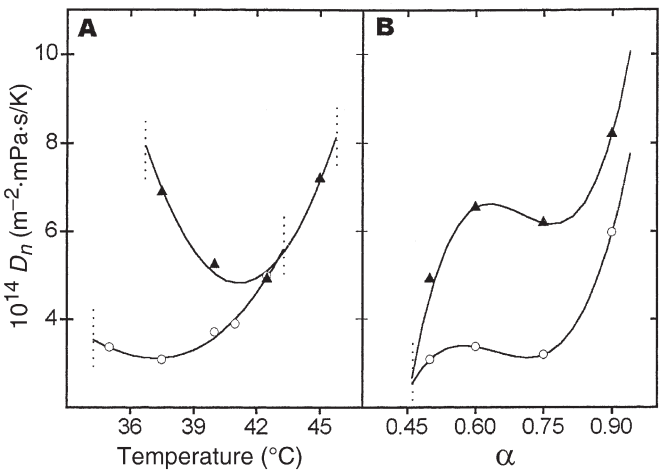

FIG. 4. Dependence of the normalized apparent diffusion coefficient, D_n, on temperature (A: at α = 0.5 and γ = 0.3) and α (B: at γ = 0.3 and T = 37.5 and 42.5°C, for BME and UPME systems, respectively). (○) BME/$C_{9/11}EO_4$/water; (▲) UPME/$C_{9/11}EO_4$/water. The vertical dotted lines show the limits of isotropic phases. For abbreviations and symbols see Figures 2 and 3.

1ϕ regions were observed and were found to be 37.5 and 42.5°C, for BME and UPME, respectively.

The dependence of D_n on α (Fig. 4B) is related to the size fluctuation of the water-rich or oil-rich domains. This shows little dependence on solution composition, in the range $\alpha \approx 0.5$–0.8. Consequently, the characteristic sizes of these domains do not vary appreciably in this range of α, consistent with the presence of bicontinuous structures (37,41,42). At $T \cong \tilde{T}$, the surfactant monolayers are almost planar, surrounded by relatively thick layers of W and O, and undulate on a short time scale. Therefore, changes in α do not appreciably affect their structures, although the thickness of water and oil domains varies (43). The increase of D_n at >0.8 is similar to that observed for systems of single components, and is due to the formation of smaller aggregates, namely W/O μE.

IFT and θ. Our IFT measurements for BME corroborate the preceding conclusion with regard to formation of bicontinuous μE in the 1ϕ regions. Interfacial tensions of both $\underline{2\phi}$ and $\overline{2\phi}$ regions were measured at different temperatures, at $\alpha = 0.5$ and $\gamma = 0.22$. The two (descending) parts of the log (IFT) vs. T plot (not shown) converge in the 1ϕ region (whose IFT is inaccessible) at *ca.* 10^{-6} mN/m^{-1}, in agreement with the formation of a bicontinuous μE (44–46). Finally, the contact angles between glass and 1ϕ regions of both oils were found to be extremely small (between 2 and 4°).

In view of the previously reported differences between phase behavior of *n*-alkanes and terminal alkenes (as oils) in systems of single components (27), the similarity between the phase diagrams and $\tilde{T}$ for CME and BME, and for SPME and UPME, is disappointing (11). Although the complexity of the present system precludes a detailed discussion of the reasons for this insensitivity to ester structure, it is possible that the expected effect of the double bond is attenuated because of its presence in the middle, not the terminus, of the ester chain. Alternatively, interactions of the polar ester group in the interfacial region (with water and/or the EO groups) are probably intense. This driving force for ester penetration into the interface leads to attenuated dependence on its structure, namely, average chain length and unsaturation. This picture is akin to intercalation of long-chain alcohols between the surfactant molecules in micellar aggregates, with the OH group "anchored" at the interfacial region (47).

Extraction Capacity of the Monophase Systems

The experimental variables are μE composition, temperature, μE/soil ratio, and contact time. The best combination of variables was arrived at as follows:

(i) Compositions. Compositions close to 1ϕ boundaries were not employed because surfactant loss by adsorption may lead to phase changes, e.g., from a 1ϕ to a 2ϕ system. From the application point of view, it is more interesting to work with μE with low surfactant and oil contents. Figure 2 shows that the lower limit of γ is *ca.* 0.2 (α constant at 0.5), so that the former ratio was varied between 0.22 and 0.40. Figures 3A and 3B show that 1ϕ regions are formed at $\alpha \geq 0.5$ (γ constant at 0.3); therefore, α was varied between 0.5 and 0.9.

(ii) Temperature. Extractions were carried out at the PIT of each W/O/S system, 37.5 and 42.5°C for BME and UPME, respectively, since decreasing the interfacial tension and/or contact angle between the soil and contaminant is crucial for its desorption and subsequent solubilization (16,17,48).

(iii) μE/soil ratio. Visually, we observed that a μE/soil ratio of 4 was insufficient to wet the whole soil. Ratios of 5 to 7 gave satisfactory results; a ratio of 6 was employed throughout.

(iv) Contact time. The decontamination rate constant was determined for silica doped with 400 ppm pyrene. This has been employed as a model soil because sample removal from the reactor and subsequent filtration of the solid could be carried out quickly (15 s), which renders kinetic studies feasible. Good pseudo first-order kinetics was observed, and the rate constant calculated, 1.1×10^{-3} s^{-1}, indicates that the extraction should be complete within *ca.* 75 min (= 7× the extraction half-life). Indeed, silica and/or bentonite contaminated with 3600 ppm pyrene was completely decontaminated after the above-mentioned contact time (see Fig. 5). The latter shows that this contact time is insufficient for cleaning contaminated soil, probably because of its high content of humic material (49,50). Therefore, we examined its decontamination as a function of contact time. At $\gamma = 0.3$ and $\alpha = 0.5$, the extraction efficiency reached a maximum after 3 h, after which it decreased. Therefore, the experiments were carried out at 3 h contact time.

Treatment of Contaminated Soil

Using this set of optimized conditions, we treated contaminated soil with μE of BME and UPME, and the results are shown in Figure 6. Considering this figure, the following points are relevant:

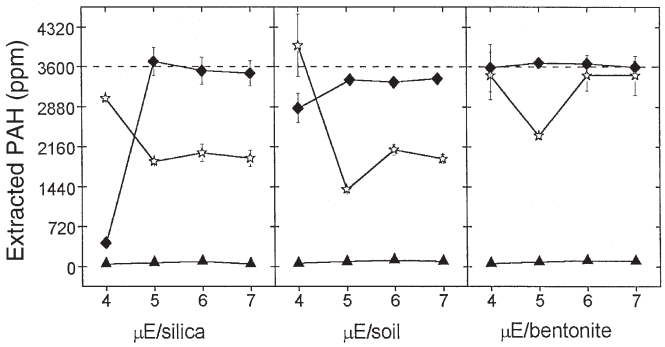

FIG. 5. Dependence of soil decontamination on μE/soil ratio at T = 37.5°C, contact time = 75 min. ◆, BME/$C_{9/11}EO_4$/water, $\alpha = 0.5$, $\gamma = 0.22$; ▲, $C_{9/11}EO_4$ aqueous solution, $\gamma = 0.22$; ☆, toluene. For brevity, we have not used "contaminated" before the name of the soil. Each point is the average of three runs. Where no vertical bars are indicated, the uncertainty limits lie within the symbol employed. The horizontal, dashed line at 3600 ppm refers to the amount extracted (6 h) with hot toluene. See Experimental Procedures section for details. PAH, polycyclic aromatic hydrocarbons; for other abbreviations see Figures 1 and 2.

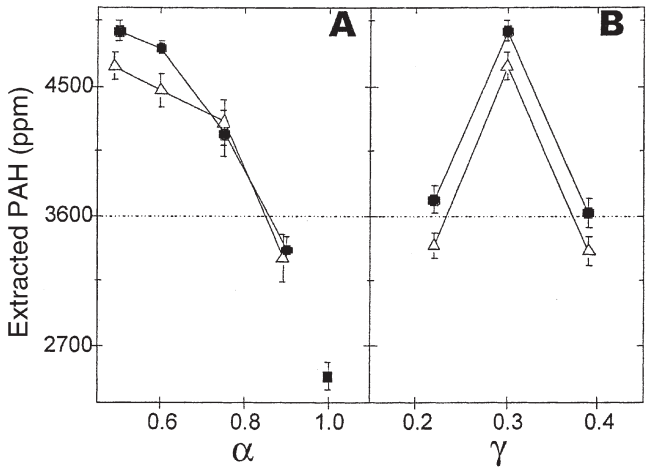

FIG. 6. Treatment of contaminated soil with μE. Contact time = 3 h, μE/soil ratio = 6. (A) γ = 0.3, (B) α = 0.5. (△) UPME/$C_{9/11}EO_4$/water, 42.5°C; (●) BME/$C_{9/11}EO_4$/water, 37.5°C. For comparison, we included the results of extraction with toluene in part A, (■), 37.5°C. The vertical lines show the uncertainty limits. The horizontal, dashed line is that defined in Figure 5. For abbreviations see Figures 1–3 and 5.

(i) Extraction capacity. The extraction capacity of these μE, at temperatures not far from room temperature, is higher than that of hot toluene. This gratifying result demonstrates the importance of very low IFT and small θ between soil and PAH for an efficient removal of the latter.

(ii) Efficiency. Extraction efficiency is clearly dependent on solution composition. Its decrease as a function of increasing α indicates that extraction by the bicontinuous phase is more efficient than, e.g., by W/O μE. As indicated above, bicontinuous phases have extremely low surface tensions and are therefore more efficient in contaminant desorption from soil. Once desorbed, the PAH stays in solution because water and oil freely mix at this solution composition.

(iii) Dependence on γ. The observed dependence on γ may be explained as follows: Soil decontamination is a dynamic process and, for certain soils, e.g., clay-rich materials, fluid–soil contact leads to new adsorption/desorption interlamellar equilibria, both for surfactant and contaminant. These equilibria depend on the conditions employed, so that the extraction efficiency may level off, or even decrease, as a function of increasing an experimental variable, e.g., contact time or solution composition (51), as shown in Figures 5 and 6.

The following results further illustrate the advantages of this decontamination scheme: (i) Favorable material balance: We have determined a material balance for BME-mediated cleaning of contaminated silica (3600 ppm pyrene). After silica removal, the μE obtained was separated into single phases; these were analyzed for individual components. The aqueous phase (88% recovery) contained 4, 20, and 84% of the initial concentrations of oil, pyrene, and surfactant, respectively. The corresponding figures for the oil phase (85% recovery) were 5.6, 80, and 8% of water, pyrene, and surfactant, respectively. The aqueous phase, containing most of the surfactant and some PAH, can be recycled into the process. Most of the pollutant is present in the oil phase; this can be appropriately discarded (e.g., by biodegradation or incineration). (ii) Better quality soil: The CEC of the decontaminated soil has a bearing on its bioavailability because of the required ion-exchange with plants. Surface charge density was determined (in mequiv/m^2) by dividing the CEC by the surface area. Decontamination by μE, with α = 0.5 and γ = 0.3, increased the original charge density of contaminated soil (0.070 mequiv/m^2) by a factor of 2.6 and 1.6 for BME and UPME, respectively.

ACKNOWLEDGMENTS

We thank the Fundação de Amparo à Pesquisa do Estado de São Paulo (FAPESP) for financial support and the Conselho Nacional de Desenvolvimento Científico e Tecnológico (CNPq) for a predoctoral fellowship to Marcia Bragato, and a research productivity fellowship to Omar A. El Seoud. We thank Prof. Milan Schwuger and Dr. Günter Subklew for their help during the initial stage of this Project, and Samuel Toffoli, Antonio C. Coelho [Escola Politécnica da Universidade de São Paulo (EP-USP)], Antonio C. Bonomi [Instituto de Pesquisas Tecnológicas (IPT)], Denise Siqueira-Petri, and Paulo A.R. Pires (Instituto de Química da Universidade de São Paulo) for their help with X-ray diffraction, BET, contact angle, and QELS measurements.

REFERENCES

1. Hamby, D.M., Site Remediation Techniques Supporting Environmental Restoration Activities—A Review, *Sci. Total Environ. 191*:203 (1996).
2. Darian, S.T., and S.P. Weinberg, WO Patent 90/06795 (1990).
3. Lee, J.F., M.M. Mortland, S.A. Boyd, and C.T. Chiou, Shape-Selective Adsorption of Aromatic Molecules from Water by Tetramethylammonium Smectite, *J. Chem. Soc., Faraday Trans. 1 85*:2953 (1989).
4. Hesketh, N., M.N. Jones, and E. Tipping, The Interaction of Some Pesticides and Herbicides with Humic Substances, *Anal. Chim. Acta 327*:191 (1996).
5. Delle Site, A., Factors Affecting Sorption of Organic Compounds in Natural Sorbent/Water Systems and Sorption Coefficients for Selected Pollutants. A Review, *J. Phys. Chem. Ref. Data 30*:187 (2001).
6. Bourbonais, K.A., G.C. Compeau, and L.K. MacClellan, Evaluating Effectiveness of *in situ* Soil Flushing with Surfactants, in *Surfactant-Enhanced Subsurface Remediation: Emerging Technologies*, edited by D.A. Sabatini, R.C. Knox, and J.H. Harwell, ACS Symposium Series, American Chemical Society, Washington, DC, 1995, Vol. 594, p. 161.
7. Bonkhoff, K., M.J. Schwuger, and G. Subklew, Use of Microemulsions for the Extraction of Contaminated Solids, in *Industrial Applications of Microemulsions*, edited by C. Solans and H. Kunieda, Surfactant Science Series, Marcel Dekker, New York, 1997, Vol. 66, p. 355.
8. Clemens, W., F.-H. Haegel, M.J. Schwuger, C. Soeder, K. Stickdorn, and L. Webb, WO Patent 94/04289 (1994).
9. Mönig, K., F.-H. Haegel, and M.J. Schwuger, Microemulsions with Plant Oils. Systematic Investigations on Preparation and Temperature-Induced Splitting, *Tenside Surfact. Deterg. 33*:228 (1996).
10. Mönig, K., W. Clemens, F.-H. Haegel, and M.J. Schwuger, Application of Microemulsions in Soil Remediation, in *Micelles, Microemulsions, and Monolayers*, edited by D.O. Shah, Marcel Dekker, New York, 1998, p. 215.
11. Bragato, M., G. Subklew, M.J. Schwuger, and O.A. El Seoud, Vegetable Oil-Based Microemulsions: Formation, Properties and Application for *"ex-situ"* Soil Decontamination, *Colloid Polym. Sci. 280*:973 (2002).

12. Perrin, D.D., and W.L.F. Armarego, *Purification of Laboratory Chemicals*, Pergamon, New York, 1988.
13. Markley, K.S., *Fatty Acids: Their Chemistry, Properties, Production and Uses*, 2nd edn., Interscience, New York, 1961, part 2.
14. Ast, H.J., Inadvertent Isomerization of Polyunsaturated Acids During Ester Preparation, *Anal. Chem. 35*:1539 (1963).
15. *Official Methods and Recommended Practices of the American Oil Chemists' Society*, 4th edn., American Oil Chemists' Society, Champaign, 1990.
16. Kahlweit, M., R. Strey, and P. Firman, Search For Tricritical Points in Ternary Systems—Water–Oil Nonionic Amphiphile, *J. Phys. Chem. 90*:671 (1986).
17. Kahlweit, M., R. Strey, D. Haase, and P. Firman, Properties of the 3-Phase Bodies in H_2O–Oil–Nonionic Amphiphile Mixtures, *Langmuir 4*:785 (1988).
18. Koppel, D.E., Analysis of Macromolecular Polydispersity in Intensity Correlation Spectroscopy—Method of Cumulants, *J. Chem. Phys. 57*:4814 (1972).
19. Evans, D.F., and H. Wennerström, *The Colloidal Domain*, VCH, New York, 1994, p. 451.
20. Kutschmann, E.-M., G.H. Findenegg, D. Nickel, and W.V. Rybinski, Interfacial Tension of Alkylglucosides in Different APG/Oil/Water Systems, *Colloid Polym. Sci. 273*:565 (1995).
21. Adamson, A., *Physical Chemistry of Surfaces*, 5th edn., John Wiley & Sons, New York, 1990, p. 389.
22. Siqueira-Petri, D.F., G. Wenz, P. Schunk, and T. Schimmel, An Improved Method for the Assembly of Amino-Terminated Monolayers on SiO_2 and the Vapor Deposition of Gold Layers, *Langmuir 15*:4520 (1999).
23. Brunauer, S., P.H. Emmett, and E. Teller, Adsorption of Gases in Multimolecular Layers, *J. Am. Chem. Soc. 60*:309 (1938).
24. Rytwo, G., C. Serban, S. Nir, and L. Margulies, Use of Methylene-Blue and Crystal Violet for Determination of Exchangeable Cations in Montmorillonite, *Clay Miner. 39*:551 (1991).
25. FAO (Food and Agriculture Organization of the United Nations), FAOSTAT Data Bank, http://apps.fao.org (accessed 2002).
26. Brazilian Institute of Geography and Statistics, IBGE, SIDRA Data-bank, www.ibge.gov.br (accessed 2002).
27. Ninham, B.W., S.J. Chen, and D.F. Evans, Role of Oils and Other Factors in Microemulsion Design, *J. Phys. Chem. 88*:5855 (1984).
28. Claesson, P.M., R. Kjellander, P. Stenius, and H.K. Christenson, *J. Chem. Soc., Faraday Trans. 1 82*:2735 (1986).
29. Golubovic, L., and T.C. Lubensky, Thermal Fluctuations and Phase-Equilibrium in Microemulsions, *Phys. Rev. A 41*:4343 (1990).
30. Schubert, K.-V., and E.W. Kaler, Nonionic Microemulsions, *Ber. Bunsen Ges. Phys. Chem. 100*:190 (1996).
31. Kunieda, H., and M. Yamagata, Mixing of Nonionic Surfactants at Water–Oil Interfaces in Microemulsions, *Langmuir 9*:3345 (1993).
32. Martino, A., M. Schick, and E.W. Kaler, A 4-Component Lattice Model for Nonaqueous Microemulsions Made with Nonionic Surfactants, *J. Chem. Phys. 93*:8228 (1990).
33. Stubenrauch, C., S.K. Mehta, B. Paeplow, and G.H. Findenegg, Microemulsion Systems Based on a C8/10 Alkyl Polyglucoside: A Reentrant Phase Inversion Induced by Alcohols? *Progr. Colloid Polym. Sci. 111*:92 (1998).
34. Yoshino, A., N. Sugiyama, H. Okabayashi, K. Taga, T. Yoshida, and O. Kamo, Chirality Effects on Proton and Carbon-13 NMR Chemical Shifts for Aerosol OT in Reverse Micelles Assisted by Line Shape Simulations and Two-Dimensional Pulse Techniques, *Colloid Surf. 67*:67 (1992).
35. Fennell Evans, D., D.J. Mitchell, and B.W. Ninham, Oil, Water, and Surfactant—Properties and Conjectured Structure of Simple Microemulsions, *J. Phys. Chem. 90*:2817 (1986).
36. De Gennes, P.G., and C. Taupin, Micro-emulsions and the Flexibility of Oil–Water Interfaces, *J. Phys. Chem. 86*:2294 (1982).
37. Tabony, J., Formation of Cubic Structures in Microemulsions Containing Equal Volumes of Oil and Water, *Nature 319*:400 (1986).
38. Tabony, J., Occurrence of Liquid-Crystalline Mesophases in Microemulsion Dispersions, *Nature 320*:338 (1986).
39. Kumar, C., and D. Balasubramamian, Spectroscopic Studies on the Microemulsions and Lamellar Phases of the System Triton X-100: Hexanol: Water in Cyclohexane, *J. Colloid Interface Sci. 69*:271 (1979).
40. Chang, N.J., and E.W. Kaler, Quasi-Elastic Light Scattering Study of Five-Component Microemulsions, *Langmuir 2*:184 (1986).
41. Kahlweit, M., R. Strey, D. Haase, H. Kunieda, T. Schmeling, B. Faulhaber, M. Borkovec, H.F. Eicke, G. Busse, F. Eggers, Th. Funck, H. Richmann, L. Magid, O. Söderman, P. Stilbs, J. Winkler, A. Dittrich, and W. Jahn, How to Study Microemulsions, *J. Colloid Interface Sci. 118*:436 (1987).
42. Talmon, Y., and S. Prager, Statistical Thermodynamics of Phase-Equilibria in Microemulsions, *J. Chem. Phys. 69*:2984 (1978).
43. Olsson, U., K. Shinoda, and B. Lindman, Change of the Structure of Microemulsions with Hydrophile-Lipophile Balance of Nonionic Surfactant as Revealed by NMR Self-Diffusion Studies, *J. Phys. Chem. 90*:4083 (1986).
44. Ruckenstein, E., Origin of Thermodynamic Stability of Emulsions, *Chem. Phys. Lett. 57*:517 (1978).
45. Testard, F., and Th. Zemb, Excess of Solubilization and Curvature in Nonionic Microemulsions, *J. Colloid Interface Sci. 219*:11 (1999).
46. Langevin, D., Microemulsions, *Accounts Chem. Res. 21*:255 (1988).
47. Zana, R., Aqueous Surfactant–Alcohol Systems—A Review, *Adv. Colloid Interface Sci. 57*:1 (1995).
48. Reed, R.L., and R.N. Healy, Contact Angles for Equilibrated Microemulsion Systems, *Soc. Petrol. Eng. J. 24*:342 (1984).
49. Johnston, C.T., Sorption of Organic Compounds on Clay Minerals: A Surface Functional Group Approach, in *Organic Pollutants in the Environment,* edited by B. Shawney, CMS Workshop Lectures, The Clay Minerals Society, Boulder, CO, 1996, Vol. 8, p. 1.
50. Rao, P.S.C., L.S. Lee, and A.L. Wood, Solubility, Sorption, and Transport of Hydrophobic Organic Chemicals in Complex Mixtures, U.S. Environmental Protection Agency Document EPA/600/M-91/009, Ada, OK, 1991.
51. Liu, Z., D.A. Edwards, and R.G. Luthy, Sorption of Nonionic Surfactants onto Soil, *Water Res. 26*:1337 (1992).

[Received June 12, 2002; accepted December 6, 2002]

Marcia Bragato obtained her M.Sc. at the Institute of Chemistry of the University of São Paulo (IQ-USP) and is now working on her Ph.D. on new low-environmental-impact polymers at the Polytechnic School of the same University (EP-USP).

Omar A. El Seoud is a professor of organic chemistry at IQ-USP. He is interested in synthesis, solution properties, and applications of surfactants, and in chemical modification of polymers and properties of their solutions.